Impact of anthropogenic climate change on wildfire across western US forests

John T. Abatzoglou[a,1] and A. Park Williams[b]

[a]Department of Geography, University of Idaho, Moscow, ID 83844; and [b]Lamont–Doherty Earth Observatory, Columbia University, Palisades, NY 10964

Edited by Monica G. Turner, University of Wisconsin–Madison, Madison, WI, and approved July 28, 2016 (received for review May 5, 2016)

Increased forest fire activity across the western continental United States (US) in recent decades has likely been enabled by a number of factors, including the legacy of fire suppression and human settlement, natural climate variability, and human-caused climate change. We use modeled climate projections to estimate the contribution of anthropogenic climate change to observed increases in eight fuel aridity metrics and forest fire area across the western United States. Anthropogenic increases in temperature and vapor pressure deficit significantly enhanced fuel aridity across western US forests over the past several decades and, during 2000–2015, contributed to 75% more forested area experiencing high (>1 σ) fire-season fuel aridity and an average of nine additional days per year of high fire potential. Anthropogenic climate change accounted for ∼55% of observed increases in fuel aridity from 1979 to 2015 across western US forests, highlighting both anthropogenic climate change and natural climate variability as important contributors to increased wildfire potential in recent decades. We estimate that human-caused climate change contributed to an additional 4.2 million ha of forest fire area during 1984–2015, nearly doubling the forest fire area expected in its absence. Natural climate variability will continue to alternate between modulating and compounding anthropogenic increases in fuel aridity, but anthropogenic climate change has emerged as a driver of increased forest fire activity and should continue to do so while fuels are not limiting.

wildfire | climate change | attribution | forests

Widespread increases in fire activity, including area burned (1, 2), number of large fires (3), and fire-season length (4, 5), have been documented across the western United States (US) and in other temperate and high-latitude ecosystems over the past half century (6, 7). Increased fire activity across western US forests has coincided with climatic conditions more conducive to wildfire (2–4, 8). The strong interannual correlation between forest fire activity and fire-season fuel aridity, as well as observed increases in vapor pressure deficit (VPD) (9), fire danger indices (10), and climatic water deficit (CWD) (11) over the past several decades, present a compelling argument that climate change has contributed to the recent increases in fire activity. Previous studies have implicated anthropogenic climate change (ACC) as a contributor to observed and projected increases in fire activity globally and in the western United States (12–19), yet no studies have quantified the degree to which ACC has contributed to observed increases in fire activity in western US forests.

Changes in fire activity due to climate, and ACC therein, are modulated by the co-occurrence of changes in land management and human activity that influence fuels, ignition, and suppression. The legacy of twentieth century fire suppression across western continental US forests contributed to increased fuel loads and fire potential in many locations (20, 21), potentially increasing the sensitivity of area burned to climate variability and change in recent decades (22). Climate influences wildfire potential primarily by modulating fuel abundance in fuel-limited environments, and by modulating fuel aridity in flammability-limited environments (1, 23, 24). We constrain our attention to climate processes that promote fuel aridity that encompass fire behavior characteristics of landscape ignitability, flammability, and fire spread via fuel desiccation in primarily flammability-limited western US forests by considering eight fuel aridity metrics that have well-established direct interannual relationships with burned area in this region (1, 8, 24, 25). Four metrics were calculated from monthly data for 1948–2015: (*i*) reference potential evapotranspiration (ETo), (*ii*) VPD, (*iii*) CWD, and (*iv*) Palmer drought severity index (PDSI). The other four metrics are daily fire danger indices calculated for 1979–2015: (*v*) fire weather index (FWI) from the Canadian forest fire danger rating system, (*vi*) energy release component (ERC) from the US national fire danger rating system, (*vii*) McArthur forest fire danger index (FFDI), and (*viii*) Keetch–Byram drought index (KBDI). These metrics are further described in the *Materials and Methods* and *Supporting Information*. Fuel aridity has been a dominant driver of regional and subregional interannual variability in forest fire area across the western US in recent decades (2, 8, 22, 25). This study capitalizes on these relationships and specifically seeks to determine the portions of the observed increase in fuel aridity and area burned across western US forests attributable to anthropogenic climate change.

The interannual variability of all eight fuel aridity metrics averaged over the forested lands of the western US correlated significantly ($R^2 = 0.57$–0.76, $P < 0.0001$; Table S1) with the logarithm of annual western US forest area burned for 1984–2015, derived from the Monitoring Trends in Burn Severity product for 1984–2014 and the Moderate Resolution Imaging Spectroradiometer (MODIS) for 2015 (*Supporting Information*). The record of standardized fuel aridity averaged across the eight metrics (hereafter, all-metric mean) accounts for 76% of the variance in the burned-area record, with significant increases in both records for 1984–2015 (Fig. 1). Correlation between fuel aridity and forest fire area remains highly significant ($R^2 = 0.72$, all-metric mean) after removing the linear-least squares trends for each time series for 1984–2015, supporting the mechanistic relationship between fuel aridity and

Significance

Increased forest fire activity across the western United States in recent decades has contributed to widespread forest mortality, carbon emissions, periods of degraded air quality, and substantial fire suppression expenditures. Although numerous factors aided the recent rise in fire activity, observed warming and drying have significantly increased fire-season fuel aridity, fostering a more favorable fire environment across forested systems. We demonstrate that human-caused climate change caused over half of the documented increases in fuel aridity since the 1970s and doubled the cumulative forest fire area since 1984. This analysis suggests that anthropogenic climate change will continue to chronically enhance the potential for western US forest fire activity while fuels are not limiting.

Author contributions: J.T.A. and A.P.W. designed research, performed research, contributed new reagents/analytic tools, analyzed data, and wrote the paper.

The authors declare no conflict of interest.

This article is a PNAS Direct Submission.

See Commentary on page 11649.

[1]To whom correspondence should be addressed. Email: jabatzoglou@uidaho.edu.

This article contains supporting information online at www.pnas.org/lookup/suppl/doi:10.1073/pnas.1607171113/-/DCSupplemental.

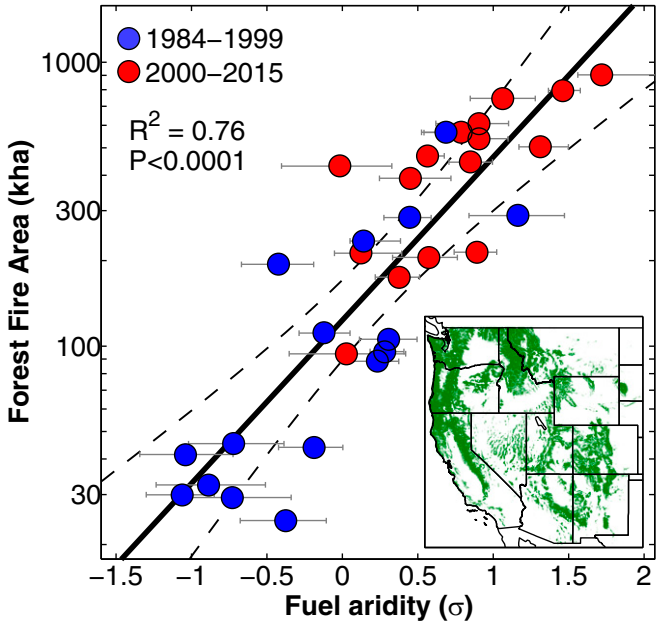

Fig. 1. Annual western continental US forest fire area versus fuel aridity: 1984–2015. Regression of burned area on the mean of eight fuel aridity metrics. Gray bars bound interquartile values among the metrics. Dashed lines bounding the regression line represent 95% confidence bounds, expanded to account for lag-1 temporal autocorrelation and to bound the confidence range for the lowest correlating aridity metric. The two 16-y periods are distinguished to highlight their 3.3-fold difference in total forest fire area. *Inset* shows the distribution of forested land across the western US in green.

forest fire area. It follows that co-occurring increases in fuel aridity and forest fire area over multiple decades would also be mechanistically related.

We quantify the influence of ACC using the Coupled Model Intercomparison Project, Phase 5 (CMIP5) multimodel mean changes in temperature and vapor pressure following Williams et al. (26) (Fig. S1; *Methods*). This approach defines the ACC signal for any given location as the multimodel mean (27 CMIP5 models) 50-y low-pass-filtered record of monthly temperature and vapor pressure anomalies relative to a 1901 baseline. Other anthropogenic effects on variables such as precipitation, wind, or solar radiation may have also contributed to changes in fuel aridity but anthropogenic contributions to these variables during our study period are less certain (22). We evaluate differences between fuel aridity metrics computed with the observational record and those computed with observations that exclude the ACC signal to determine the contribution of ACC to fuel aridity. To exclude the ACC signal, we subtract the ACC signal from daily and monthly temperature and vapor pressure, leaving all other variables unchanged and preserving the temporal variability of observations. The contribution of ACC to changes in fuel aridity is shown for the entire western United States; however, we constrain the focus of our attribution and analysis to forested environments of the western US (Fig. 1, *Inset*; *Methods*).

Anthropogenic increases in temperature and VPD contributed to a standardized (σ) increase in all-metric mean fuel aridity averaged for forested regions of +0.6 σ (range of +0.3 σ to +1.1 σ across all eight metrics) for 2000–2015 (Fig. 2). We found similar results with reanalysis products (all-metric mean fuel aridity increase of +0.6 σ for two reanalysis datasets considered; *Methods*), suggesting robustness of the results to structural uncertainty in observational products (Figs. S2–S4 and Table S2). The largest anthropogenic increases in standardized fuel aridity were present across the intermountain western United States, due in part to larger modeled warming rates relative to more maritime areas (27). Among aridity metrics, the largest increases tied to the ACC signal were for VPD and ETo because the interannual variability of these variables is primarily driven by temperature for much of the study area (28). By contrast, PDSI and ERC showed more subdued ACC driven increases in fuel aridity because these metrics are more heavily influenced by precipitation variability.

Fuel aridity averaged across western US forested areas showed a significant increase over the past three decades, with a linear trend of +1.2 σ (95% confidence: 0.42–2.0 σ) in the all-metric mean for 1979–2015 (Fig. 3*A*, *Top* and Table S1). The all-metric mean ACC contribution since 1901 was +0.10 σ by 1979 and +0.71 σ by 2015. The annual area of forested lands with high fuel aridity (>1 σ) increased significantly during 1948–2015, most notably since 1979 (Fig. 3*A*, *Bottom*). The observed mean annual areal extent of forested land with high aridity during 2000–2015 was 75% larger for the all-metric mean (+27% to +143% range across metrics) than was the case where the ACC signal was excluded.

Significant positive trends in fuel aridity for 1979–2015 across forested lands were observed for all metrics (Fig. 3*B* and Table S1). Positive trends in fuel aridity remain after excluding the ACC signal, but the remaining trend was only significant for ERC. Anthropogenic forcing accounted for 55% of the observed positive trend in the all-metric mean fuel aridity during 1979–2015, including at least two-thirds of the observed increase in ETo, VPD, and FWI, and less than a third of the observed increase in ERC and PDSI. No significant trends were observed for monthly fuel aridity metrics from 1948–1978.

The duration of the fire-weather season increased significantly across western US forests (+41%, 26 d for the all-metric mean) during 1979–2015, similar to prior results (10) (Fig. 4*A* and Table S2). Our analysis shows that ACC accounts for ~54% of the increase in fire-weather season length in the all-metric mean (15–79% for individual metrics). An increase of 17.0 d per year of high fire potential was observed for 1979–2015 in the all-metric mean (11.7–28.4 d increase for individual metrics), over twice the rate of increase calculated from metrics that excluded the ACC signal (Fig. 4*B* and Table S2). This translates to an average of an additional 9 d (7.8–12.0 d) per year of high fire potential during 2000–2015 due to ACC.

Given the strong relationship between fuel aridity and annual western US forest fire area, and the detectable impact of ACC on fuel aridity, we use the regression relationship in Fig. 1 to model

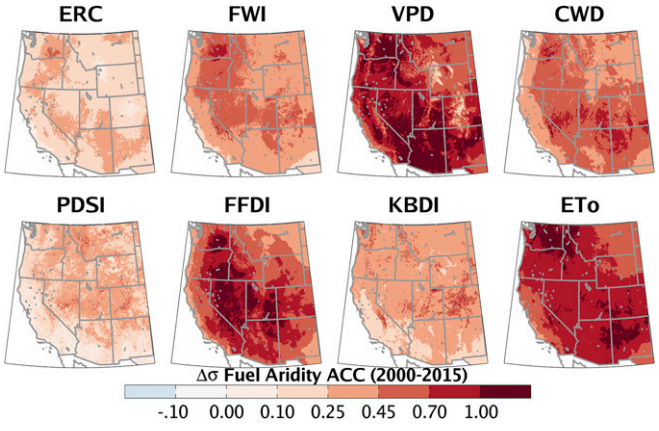

Fig. 2. Standardized change in each of the eight fuel aridity metrics due to ACC. The influence of ACC on fuel aridity during 2000–2015 is shown by the difference between standardized fuel aridity metrics calculated from observations and those calculated from observations excluding the ACC signal. The sign of PDSI is reversed for consistency with other aridity measures.

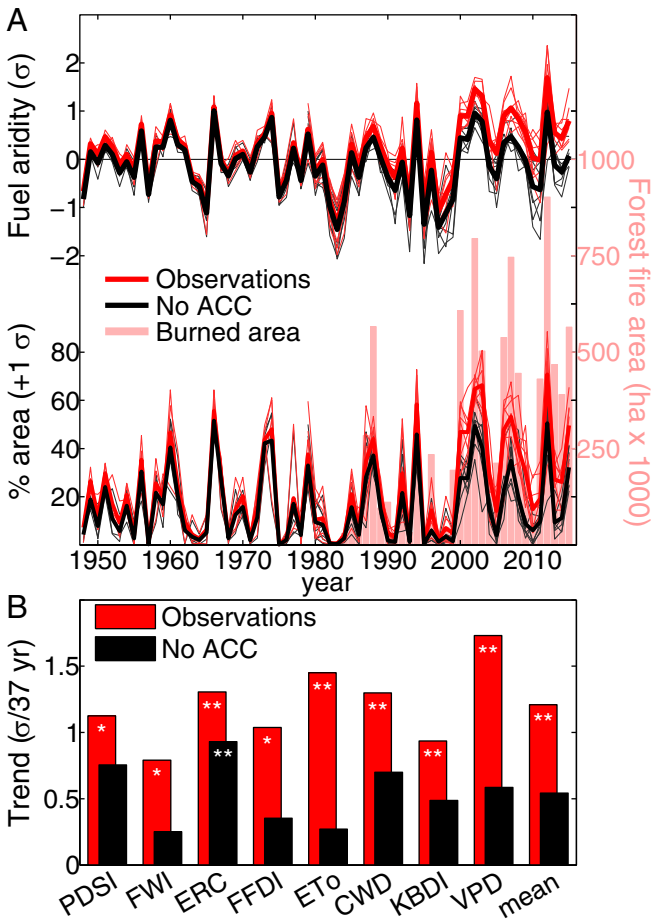

Fig. 3. Evolution and trends in western US forest fuel aridity metrics over the past several decades. (*A*) Time series of (*Upper*) standardized annual fuel aridity metrics and (*Lower*) percent of forest area with standardized fuel aridity exceeding one SD. Red lines show observations and black lines show records after exclusion of the ACC signal. Only the four monthly metrics extend back to 1948. Daily fire danger indices begin in 1979. Bold lines indicate averages across fuel aridity metrics. Bars in the background of *A* show annual forested area burned during 1984–2015 for visual comparison with fuel aridity. (*B*) Linear trends in the standardized fuel aridity metrics during 1979–2015 for (red) observations and (black) records excluding the ACC signal (differences attributed to ACC). Asterisks indicate positive trends at the (*) 95% and (**) 99% significance levels.

the contribution of ACC on western US forest fire area for the past three decades (Fig. 5 and Fig. S5). ACC-driven increases in fuel aridity are estimated to have added ∼4.2 million ha (95% confidence: 2.7–6.5 million ha) of western US forest fire area during 1984–2015, similar to the combined areas of Massachusetts and Connecticut, accounting for nearly half of the total modeled burned area derived from the all-metric mean fuel aridity. Repeating this calculation for individual fuel aridity metrics yields ACC contributions of 1.9–4.9 million ha, but most individual fuel aridity metrics had weaker correlations with burned area and thus may be less appropriate proxies for attributing burned area. The effect of the ACC forcing on fuel aridity increased during this period, contributing ∼5.0 (95% confidence: 4.2–5.9) times more burned area in 2000–2015 than in 1984–1999 (Fig. 5*B*). During 2000–2015, the ACC-forced burned area likely exceeded the burned area expected in the absence of ACC (Fig. 5*B*). A more conservative method that uses the relationship between detrended records of burned area and fuel aridity (2) still indicates a substantial impact of ACC on total burned area, with a 19% (95% confidence: 12–24%) reduction in the proportion of total burned area attributable to ACC (Fig. S5).

Our attribution explicitly assumes that anthropogenic increases in fuel aridity are additive to the wildfire extent that would have arisen from natural climate variability during 1984–2015. Because the influence of fuel aridity on burned area is exponential, the influence of a given ACC forcing is larger in an already arid fire season such as 2012 (Fig. 5*A* and Fig. S5*C*). Anthropogenic increases in fuel aridity are expected to continue to have their most prominent impacts when superimposed on naturally occurring extreme climate anomalies. Although numerous studies have projected changes in burned area over the twenty-first century due to ACC, we are unaware of other studies that have attempted to quantify the contribution of ACC to recent forested burned area over the western United States. The near doubling of forested burned area we attribute to ACC exceeds changes in burned area projected by some modeling efforts to occur by the mid-twenty-first century (29, 30), but is proportionally consistent with mid-twenty-first century increases in burned area projected by other modeling efforts (17, 31–33).

Beyond anthropogenic climatic changes, several additional factors have caused increases in fuel aridity and forest fire area since the 1970s. The lack of fuel aridity trends during 1948–1978 and persistence of positive trends during 1979–2015 even after removing the ACC signal implicates natural multidecadal climate variability as an important factor that buffered anthropogenic

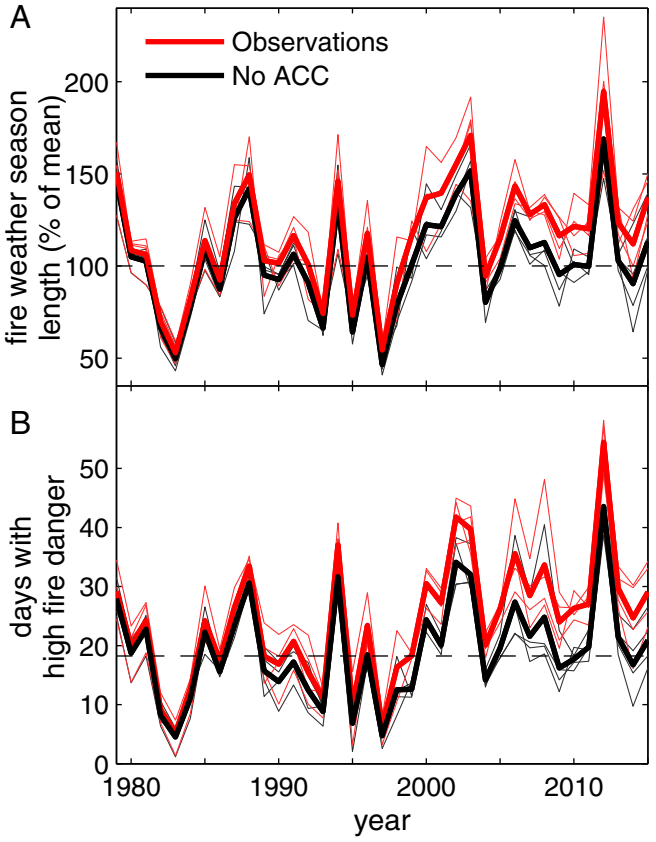

Fig. 4. Changes in fire-weather season length and number of high fire danger days. Time series of mean western US forest (*A*) fire-weather season length and (*B*) number of days per year when daily fire danger indices exceeded the 95th percentile. Baseline period: 1981–2010 using observational records that exclude the ACC signal. Red lines show the observed record, and black lines show the record that excludes the ACC signal. Bold lines show the average signal expressed across fuel aridity metrics.

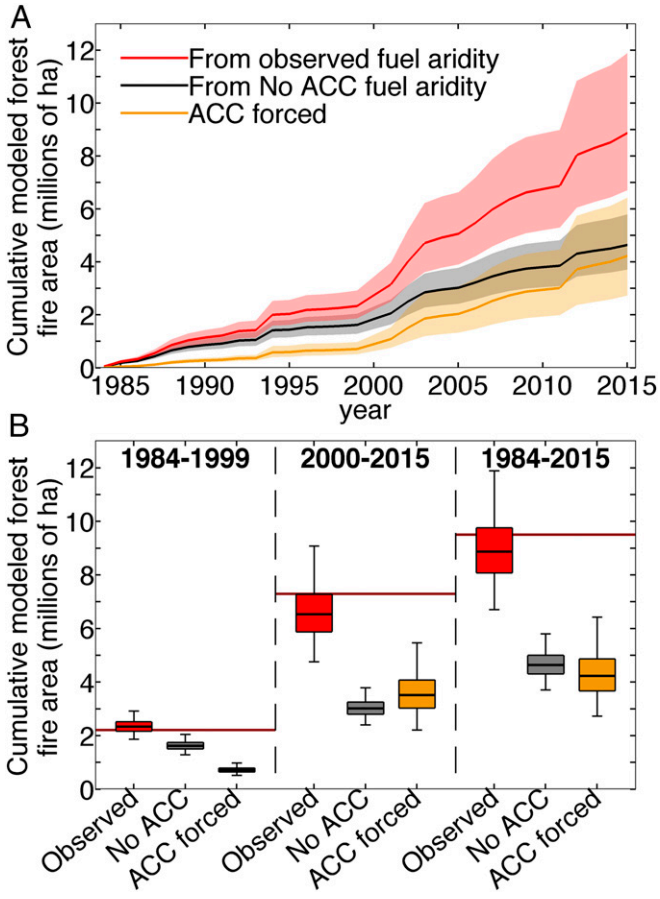

Fig. 5. Attribution of western US forest fire area to ACC. Cumulative forest fire area estimated from the (red) observed all-metric mean record of fuel aridity and (black) the fuel aridity record after exclusion of ACC (No ACC). The (orange) difference is the forest fire area forced by anthropogenic increases in fuel aridity. Bold lines in *A* and horizontal lines within box plots in *B* indicate mean estimated values (regression values in Fig. 1). Boxes in *B* bound 50% confidence intervals. Shaded areas in *A* and whiskers in *B* bound 95% confidence intervals. Dark red horizontal lines in *B* indicate observed forest fire area during each period.

effects during 1948–1978 and compounded anthropogenic effects during 1979–2015. During 1979–2015, for example, observed Mar–Sep vapor pressure decreased significantly across many US forest areas, in marked contrast to modeled anthropogenic increases (Fig. S6) (34). Significant declines in spring (Mar–May) precipitation in the southwestern United States and summer (Jun–Sep) precipitation throughout parts of the northwestern United States during 1979–2015 (Fig. S7 *A* and *B*) hastened increases in fire-season fuel aridity, consistent with observed increases in the number of consecutive dry days across the region (10). Natural climate variability, including a shift toward the cold phase of the interdecadal Pacific Oscillation (35), was likely the dominant driver of observed regional precipitation trends (36) (Fig. S7 *B* and *D*).

Our quantification of the ACC contribution to observed increases in forest fire activity in the western United States adds to the limited number of climate change attribution studies on wildfire to date (37). Previous attribution efforts have been restricted to a single GCM and biophysical variable (14, 16). We complement these studies by demonstrating the influence of ACC derived from an ensemble of GCMs on several biophysical metrics that exhibit strong links to forest fire area. However, our attribution effort only considers ACC to manifest as trends in mean climate conditions, which may be conservative because climate models also project anthropogenic increases in the temporal variability of climate and drought in the western United States (34, 38, 39). In focusing exclusively on the direct impacts of ACC on fuel aridity, we do not address several other pathways by which ACC may have affected wildfire activity. For example, the fuel aridity metrics that we used may not adequately capture the role of mountain snow hydrology on soil moisture. Nor do we account for the influence of climate change on lightning activity, which may increase with warming (40). We also do not account for how fire risk may be affected by changes in biomass/fuel due to increases in atmospheric CO_2 (41), drought-induced vegetation mortality (42), or insect outbreaks (43).

Additionally, we treat the impact of ACC on fire as independent from the effects of fire management (e.g., suppression and wildland fire use policies), ignitions, land cover (e.g., exurban development), and vegetation changes beyond the degree to which they modulate the relationship between fuel aridity and forest fire area. These factors have likely added to the area burned across the western US forests and potentially amplified the sensitivity of wildfire activity to climate variability and change in recent decades (2, 22, 24, 44). Such confounding influences, along with nonlinear relationships between burned area and its drivers (e.g., Fig. 1), contribute uncertainty to our empirical attribution of regional burned area to ACC. Our approach depends on the strong observed regional relationship between burned area and fuel aridity at the large regional scale of the western United States, so the quantitative results of this attribution effort are not necessarily applicable at finer spatial scales, for individual fires, or to changes in nonforested areas. Dynamical vegetation models with embedded fire models show emerging promise as tools to diagnose the impacts of a richer set of processes than those considered here (41, 45) and could be used in tandem with empirical approaches (46, 47) to better understand contributions of observed and projected ACC to changes in regional fire activity. However, dynamic models of vegetation, human activities, and fire are not without their own lengthy list of caveats (2). Given the strong empirical relationship between fuel aridity and wildfire activity identified here and in other studies (1, 2, 4, 8), and substantial increases in western US fuel aridity and fire-weather season length in recent decades, it appears clear from empirical data alone that increased fuel aridity, which is a robustly modeled result of ACC, is the proximal driver of the observed increases in western US forest fire area over the past few decades.

Conclusions

Since the 1970s, human-caused increases in temperature and vapor pressure deficit have enhanced fuel aridity across western continental US forests, accounting for approximately over half of the observed increases in fuel aridity during this period. These anthropogenic increases in fuel aridity approximately doubled the western US forest fire area beyond that expected from natural climate variability alone during 1984–2015. The growing ACC influence on fuel aridity is projected to increasingly promote wildfire potential across western US forests in the coming decades and pose threats to ecosystems, the carbon budget, human health, and fire suppression budgets (13, 48) that will collectively encourage the development of fire-resilient landscapes (49). Although fuel limitations are likely to eventually arise due to increased fire activity (17), this process has not yet substantially disrupted the relationship between western US forest fire area and aridity. We expect anthropogenic climate change and associated increases in fuel aridity to impose an increasingly dominant and detectable effect on western US forest fire area in the coming decades while fuels remain abundant.

Methods

We focus on climate variables that directly affect fuel moisture over forested areas of the western continental United States, where fire activity tends to be flammability-limited rather than fuel- or ignition-limited (1) (study region shown in Fig. 1, *Inset*). There are a variety of climate-based metrics that have been used as proxies for fuel aridity, yet there is no universally preferred metric across different vegetation types (24). We consider eight frequently used fuel aridity metrics that correlate well with fire activity variables, including annual burned area (Fig. 1 and Table S1), in western US forests.

Fuel aridity metrics are calculated from daily surface meteorological data (50) on a 1/24° grid for 1979–2015 for the western United States (west of 103°W). Although we calculated metrics across the entire western United States, we focus on forested lands defined by the climax succession vegetation stages of "forest" or "woodland" in the Environmental Site Potential product of LANDFIRE (landfire.gov). Forested 1/24° grid cells are defined by at least 50% forest coverage aggregated from LANDFIRE. We extended the aridity metrics calculated at the monthly timescale (ETo, VPD, CWD, and PDSI) back to 1948 using monthly anomalies relative to a common 1981–2010 period from the dataset developed by the Parameterized Regression on Independent Slopes Model group (51) for temperature, precipitation, and vapor pressure, and by bilinearly interpolating NCEP–NCAR reanalysis for wind speed and surface solar radiation. We aggregated data to annualized time series of mean May–Sep daily FWI, KBDI, ERC, and FFDI; Mar–Sep VPD and ETo; Jun–Aug PDSI; and Jan–Dec CWD. We also calculated the aridity metrics strictly from ERA-INTERIM and NCEP–NCAR reanalysis products for 1979–2015 covering the satellite era (*Supporting Information*).

Days per year of high fire potential are quantified by daily fire danger indices (ERC, FWI, FFDI, and KBDI) that exceed the 95th percentile threshold defined during 1981–2010 from observations after removing the ACC signal. Observational studies have shown that fire growth preferentially occurs during high fire danger periods (52, 53). We also calculate the fire weather season length for the four daily fire danger indices following previous studies (10).

The ACC signal is obtained from ensemble members taken from 27 CMIP5 global climate models (GCMs) regridded to a common 1° resolution for 1850–2005 using historical forcing experiments and for 2006–2099 using the Representative Concentration Pathway (RCP) 8.5 emissions scenario (Table S3 and *Supporting Information*). These GCMs were selected based on availability of monthly outputs for maximum and minimum daily temperature (T_{max} and T_{min}, respectively), specific humidity (*huss*), and surface pressure. Saturation vapor pressure (e_s), vapor pressure (e), and VPD were calculated using standard methods (*Supporting Information*). A variety of approaches exist to estimate the ACC signal (26). We define the anthropogenic signals in T_{max}, T_{min}, e, e_s, VPD, and relative humidity by a 50-y low-pass-filter time series (using a 10-point Butterworth filter) averaged across the 27 GCMs using the following methodology: For each GCM, variable, month, and grid cell, we converted each annual time series to anomalies relative to a 1901–2000 baseline. We averaged annual anomalies across all realizations (model runs) for each GCM and calculated a single 50-y low-pass-filter annual time series for each of the 12 mo for 1850–2099. We averaged each month's low-pass-filtered time series across the 27 GCMs and additively adjusted so that all smoothed records pass through zero in 1901. The resultant ACC signal represents the CMIP5 modeled anthropogenic impact since 1901 for each variable, grid cell, and month (*Supporting Information*).

We bilinearly interpolated the 1° CMIP5 multimodel mean 50-y low-pass time series to the 1/24° spatial resolution of the observations and subtracted the ACC signal from the observed daily and monthly time series. We consider the remaining records after subtraction of the ACC signal to indicate climate records that are free of anthropogenic trends (26).

Annual variations in fuel aridity metrics are presented as standardized anomalies (σ) to accommodate differences across geography and metrics. All fuel aridity metrics are standardized using the mean and SD from 1981 to 2010 for observations that excluded the ACC signal. Although the selection of a reference period can bias results (54), our findings were similar when using the full 1979–2015 time period or the observed data (without removal of ACC) for the reference period. The influence of anthropogenic forcing on fuel aridity metrics is quantified as the difference between metrics calculated with observations and those calculated with observations that excluded the ACC signal. Area-weighted standardized anomalies and the spatial extent of western US forested land that experienced high (>1 σ) aridity are computed for each aridity metric. Annualized burned area as well as aggregated fuel aridity metrics calculated with data from ref. 50 and the two reanalysis products are provided in Datasets S1–S3.

We use the regression relationship between the annual western US forest fire area and the all-metric mean fuel aridity index in Fig. 1 to estimate the forcing of anthropogenic increases in fuel aridity on forest fire area during 1984–2015. Uncertainties in the regression relationship due to imperfect correlation and temporal autocorrelation are propagated as estimated confidence bounds on the anthropogenic forcing of forest fire area. This approach was repeated using a more conservative definition of the regression relationship, where we removed the linear least squares trend for 1984–2015 from both the area burned and fuel aridity time series before regression to reduce the possibility of spurious correlation due to common but unrelated trends (Fig. S5). Statistical significance of all linear trends and correlations reported in this study are assessed using both Spearman's rank and Kendall's tau statistics. Trends are considered significant if both tests yield $P < 0.05$.

ACKNOWLEDGMENTS. We thank J. Mankin, B. Osborn, and two reviewers for helpful comments on the manuscript and coauthors of ref. 26 for help developing the empirical attribution framework. A.P.W. was funded by Columbia University's Center for Climate and Life and by the Lamont-Doherty Earth Observatory (Lamont contribution 8048). J.T.A. was supported by funding from National Aeronautics and Space Administration Terrestrial Ecology Program under Award NNX14AJ14G, and the National Science Foundation Hazards Science, Engineering and Education for Sustainability (SEES) Program under Award 1520873.

1. Littell JS, McKenzie D, Peterson DL, Westerling AL (2009) Climate and wildfire area burned in western U.S. ecoprovinces, 1916-2003. *Ecol Appl* 19(4):1003–1021.
2. Williams AP, Abatzoglou JT (2016) Recent advances and remaining uncertainties in resolving past and future climate effects on global fire activity. *Curr Clim Chang Reports* 2:1–14.
3. Dennison P, Brewer S, Arnold J, Moritz M (2014) Large wildfire trends in the western United States, 1984–2011. *Geophys Res Lett* 41:2928–2933.
4. Westerling AL, Hidalgo HG, Cayan DR, Swetnam TW (2006) Warming and earlier spring increase western U.S. forest wildfire activity. *Science* 313(5789):940–943.
5. Westerling AL (2016) Increasing western US forest wildfire activity: Sensitivity to changes in the timing of spring. *Philos Trans R Soc B Biol Sci* 371(1696):20150178.
6. Kasischke ES, Turetsky MR (2006) Recent changes in the fire regime across the North American boreal region - Spatial and temporal patterns of burning across Canada and Alaska. *Geophys Res Lett* 33(9):L09703.
7. Kelly R, et al. (2013) Recent burning of boreal forests exceeds fire regime limits of the past 10,000 years. *Proc Natl Acad Sci USA* 110(32):13055–13060.
8. Abatzoglou JT, Kolden CA (2013) Relationships between climate and macroscale area burned in the western United States. *Int J Wildland Fire* 22(7):1003–1020.
9. Seager R, et al. (2015) Climatology, variability, and trends in the U.S. vapor pressure deficit, an important fire-related meteorological quantity. *J Appl Meteorol Climatol* 54(6):1121–1141.
10. Jolly WM, et al. (2015) Climate-induced variations in global wildfire danger from 1979 to 2013. *Nat Commun* 6:7537.
11. Dobrowski SZ, et al. (2013) The climate velocity of the contiguous United States during the 20th century. *Glob Change Biol* 19(1):241–251.
12. Flannigan MD, Krawchuk MA, de Groot WJ, Wotton BM, Gowman LM (2009) Implications of changing climate for global wildland fire. *Int J Wildland Fire* 18(5):483–507.
13. Flannigan M, et al. (2013) Global wildland fire season severity in the 21st century. *For Ecol Manage* 294:54–61.
14. Yoon J, Kravitz B, Rasch P (2015) Extreme fire season in California: A glimpse into the future? *Bull Am Meteorol Soc* 96:S5–S9.
15. Barbero R, Abatzoglou JT, Larkin NK, Kolden CA, Stocks B (2015) Climate change presents increased potential for very large fires in the contiguous United States. *Int J Wildland Fire* 24(7):892–899.
16. Gillett NP, Weaver AJ, Zwiers FW, Flannigan MD (2004) Detecting the effect of climate change on Canadian forest fires. *Geophys Res Lett* 31(18):L18211.
17. Westerling AL, Turner MG, Smithwick EAH, Romme WH, Ryan MG (2011) Continued warming could transform Greater Yellowstone fire regimes by mid-21st century. *Proc Natl Acad Sci USA* 108(32):13165–13170.
18. Krawchuk MA, Moritz MA, Parisien MA, Van Dorn J, Hayhoe K (2009) Global pyrogeography: The current and future distribution of wildfire. *PLoS One* 4(4):e5102.
19. Moritz MA, et al. (2012) Climate change and disruptions to global fire activity. *Ecosphere* 3(6):1–22.
20. Marlon JR, et al. (2012) Long-term perspective on wildfires in the western USA. *Proc Natl Acad Sci USA* 109(9):E535–E543.
21. Parks SA, et al. (2015) Wildland fire deficit and surplus in the western United States, 1984–2012. *Ecosphere* 6(12):1–13.
22. Higuera PE, Abatzoglou JT, Littell JS, Morgan P (2015) The changing strength and nature of fire–climate relationships in the northern Rocky Mountains, U.S.A., 1902-2008. *PLoS One* 10(6):e0127563.
23. Pausas JG, Ribeiro E (2013) The global fire–productivity relationship. *Glob Ecol Biogeogr* 22(6):728–736.
24. Littell JS, Peterson DL, Riley KL, Liu Y, Luce CH (2016) A review of the relationships between drought and forest fire in the United States. *Glob Change Biol* 22(7): 2353–2369.

25. Williams AP, et al. (2015) Correlations between components of the water balance and burned area reveal new insights for predicting forest fire area in the southwest United States. *Int J Wildland Fire* 24(1):14–26.
26. Williams AP, et al. (2015) Contribution of anthropogenic warming to California drought during 2012–2014. *Geophys Res Lett* 42(16):6819–6828.
27. Sheffield J, et al. (2013) North American Climate in CMIP5 experiments. Part I: Evaluation of historical simulations of continental and regional climatology. *J Clim* 26(23): 9209–9245.
28. Hobbins MT (2016) The variability of ASCE standardized reference evapotranspiration: A rigorous, CONUS-wide decomposition and attribution. *Trans Am Soc Agric Biol Eng* 59(2):561–576.
29. Mann ML, et al. (2016) Incorporating anthropogenic influences into fire probability models: Effects of human activity and climate change on fire activity in California. *PLoS One* 11(4):e0153589.
30. Yue X, Mickley LJ, Logan JA, Kaplan JO (2013) Ensemble projections of wildfire activity and carbonaceous aerosol concentrations over the western United States in the mid-21st century. *Atmos Environ (1994)* 77:767–780.
31. Pechony O, Shindell DT (2010) Driving forces of global wildfires over the past millennium and the forthcoming century. *Proc Natl Acad Sci USA* 107(45):19167–19170.
32. Littell JS, et al. (2010) Forest ecosystems, disturbance, and climatic change in Washington State, USA. *Clim Change* 102(1-2):129–158.
33. Rogers BM, et al. (2011) Impacts of climate change on fire regimes and carbon stocks of the U.S. Pacific Northwest. *J Geophys Res Biogeosci* 116(G3):G03037.
34. Williams AP, et al. (2014) Causes and implications of extreme atmospheric moisture demand during the record-breaking 2011 wildfire season in the southwestern United States. *J Appl Meteorol Climatol* 53(12):2671–2684.
35. Dong B, Dai A (2015) The influence of the Interdecadal Pacific Oscillation on temperature and precipitation over the globe. *Clim Dyn* 45(9-10):2667–2681.
36. Deser C, Knutti R, Solomon S, Phillips AS (2012) Communication of the role of natural variability in future North American climate. *Nat Clim Chang* 2(11):775–779.
37. National Academies of Sciences, Engineering, and Medicine (2016) *Attribution of Extreme Weather Events in the Context of Climate Change* (The National Academies Press, Washington, DC).
38. Swain DL, Horton DE, Singh D, Diffenbaugh NS (2016) Trends in atmospheric patterns conducive to seasonal precipitation and temperature extremes in California. *Sci Adv* 2(4):e1501344.
39. Polade SD, Pierce DW, Cayan DR, Gershunov A, Dettinger MD (2014) The key role of dry days in changing regional climate and precipitation regimes. *Sci Rep* 4:4364.
40. Romps DM, Seeley JT, Vollaro D, Molinari J (2014) Climate change. Projected increase in lightning strikes in the United States due to global warming. *Science* 346(6211): 851–854.
41. Knorr W, Jiang L, Arneth A (2016) Climate, CO_2 and human population impacts on global wildfire emissions. *Biogeosciences* 13(1):267–282.
42. Williams AP, et al. (2013) Temperature as a potent driver of regional forest drought stress and tree mortality. *Nat Clim Chang* 3(3):292–297.
43. Hart SJ, Schoennagel T, Veblen TT, Chapman TB (2015) Area burned in the western United States is unaffected by recent mountain pine beetle outbreaks. *Proc Natl Acad Sci USA* 112(14):4375–4380.
44. Van Wagtendonk JW (2007) The history and evolution of wildland fire use. *Fire Ecol* 3(2):3–17.
45. Bowman DMJS, Murphy BP, Williamson GJ, Cochrane MA (2014) Pyrogeographic models, feedbacks and the future of global fire regimes. *Glob Ecol Biogeogr* 23(7): 821–824.
46. Parisien M-A, et al. (2014) An analysis of controls on fire activity in boreal Canada: Comparing models built with different temporal resolutions. *Ecol Appl* 24(6):1341–1356.
47. Krawchuk MA, Moritz MA (2014) Burning issues: Statistical analyses of global fire data to inform assessments of environmental change. *Environmetrics* 25(6):472–481.
48. Millar CI, Stephenson NL (2015) Temperate forest health in an era of emerging megadisturbance. *Science* 349(6250):823–826.
49. Smith AMS, et al. (2016) The science of firescapes: Achieving fire-resilient communities. *Bioscience* 66(2):130–146.
50. Abatzoglou JT (2013) Development of gridded surface meteorological data for ecological applications and modelling. *Int J Climatol* 33(1):121–131.
51. Daly C, et al. (2008) Physiographically sensitive mapping of climatological temperature and precipitation across the conterminous United States. *Int J Climatol* 28(15): 2031–2064.
52. Stavros EN, Abatzoglou J, Larkin NK, McKenzie D, Steel EA (2014) Climate and very large wildland fires in the contiguous Western USA. *Int J Wildland Fire* 23(7):899–914.
53. Riley KL, Abatzoglou JT, Grenfell IC, Klene AE, Heinsch FA (2013) The relationship of large fire occurrence with drought and fire danger indices in the western USA, 1984–2008: The role of temporal scale. *Int J Wildland Fire* 22(7):894–909.
54. Sippel S, et al. (2015) Quantifying changes in climate variability and extremes: Pitfalls and their overcoming. *Geophys Res Lett* 42(22):9990–9998.
55. Littell JS, Gwozdz RB (2011) Climatic water balance and regional fire years in the Pacific Northwest, USA: linking regional climate and fire at landscape scales. *The Landscape Ecology of Fire* (Springer, Dordrecht, The Netherlands), pp 117–139.
56. Morton DC, et al. (2013) Satellite-based assessment of climate controls on US burned area. *Biogeosciences* 10(1):247–260.
57. Stocks BJ, et al. (1989) Canadian forest fire danger rating system: An overview. *For Chron* 65(4):258–265.
58. Westerling AL, Gershunov A, Brown TJ, Cayan DR, Dettinger MD (2003) Climate and wildfire in the western United States. *Bull Am Meteorol Soc* 84(5):595–604.
59. Flannigan MD, et al. (2016) Fuel moisture sensitivity to temperature and precipitation: Climate change implications. *Clim Change* 134(1-2):59–71.
60. Flannigan MD, Van Wagner CE (1991) Climate change and wildfire in Canada. *Can J Res* 21(1):66–72.
61. Dowdy AJ, Mills GA, Finkele K, de Groot W (2010) Index sensitivity analysis applied to the Canadian Forest Fire Weather Index and the McArthur Forest Fire Danger Index. *Meteorol Appl* 17(3):298–312.
62. Mitchell KE, et al. (2004) The multi-institution North American Land Data Assimilation System (NLDAS): Utilizing multiple GCIP products and partners in a continental distributed hydrological modeling system. *J Geophys Res Atmos* 109(D7):D07S90.
63. Allen RG, Pereira LS, Raes D, Smith M (1998) Crop evapotranspiration-Guidelines for computing crop water requirements-FAO Irrigation and drainage paper 56. *FAO, Rome* 300(9):D05109.
64. Willmott CJ, Rowe CM, Mintz Y (1985) Climatology of the terrestrial seasonal water cycle. *J Climatol* 5(6):589–606.
65. Andrews PL, Loftsgaarden DO, Bradshaw LS (2003) Evaluation of fire danger rating indexes using logistic regression and percentile analysis. *Int J Wildland Fire* 12(2): 213–226.
66. Cohen JE, Deeming JD (1985) The National Fire-Danger Rating System: basic equations. *Gen Tech Rep*:16.
67. McArthur AG (1967) *Fire behaviour in eucalypt forests* (Forestry and Timber Bureau Leaflet 107).
68. Griffiths D (1999) Improved formula for the drought factor in McArthur's Forest Fire Danger Meter. *Aust For* 62(3):202–206.
69. Wallace JM, Hobbs PV (2006) *Atmospheric Science: An Introductory Survey* (Academic, Amsterdam), 2nd Ed.
70. Eidenshink JC, et al. (2007) A project for monitoring trends in burn severity. *Fire Ecol* 3(1):3–21.
71. Roy DP, Boschetti L, Justice CO, Ju J (2008) The collection 5 MODIS burned area product—Global evaluation by comparison with the MODIS active fire product. *Remote Sens Environ* 112(9):3690–3707.
72. van Vuuren DP, et al. (2011) The representative concentration pathways: An overview. *Clim Change* 109(1):5–31.

Supporting Information

Abatzoglou and Williams 10.1073/pnas.1607171113

Fuel Aridity Metrics

We use eight metrics as proxies for fuel aridity that have established interannual links to area burned in forested systems: (*i*) reference evapotranspiration (ETo) (55, 56), (*ii*) vapor pressure deficit (VPD) (25), (*iii*) fire weather index (FWI) from the Canadian forest fire danger rating system (57), (*iv*) energy release component (ERC) from the US national fire danger rating system (8), (*v*) climatic water deficit (CWD) (17), (*vi*) McArthur forest fire danger index (FFDI) (10), (*vii*) Keetch–Byram drought index (KBDI) (25), and (*viii*) Palmer drought severity index (PDSI) (58). Each metric varies in terms of its input requirements, serial correlation, and sensitivity to the driving meteorological fields (59–61).

Daily surface meteorological data from ref. 50 are used to calculate the fuel aridity metrics. These data combine the temporal attributes and multiple variables from the North American Land Data Assimilation System 2 meteorological forcing dataset (NLDAS2; ref. 62) and the spatial attributes of the monthly dataset developed by the Parameterized Regression on Independent Slopes Model (PRISM) group at Oregon State University (51).

Monthly climate data are used to calculate PDSI, ETo, CWD, and VPD. We calculate ETo using the Penman–Monteith method (63). PDSI is calculated using monthly ETo, precipitation, and soil water holding capacity derived from State Soil Geographic (STATGO) database and aggregated to the 1/24° grid (26). CWD is calculated using a monthly water balance runoff model that has been modified to account for snowpack dynamics (11, 64).

Monthly mean vapor pressure (e) is estimated from monthly mean specific humidity and an estimate of surface pressure based on elevation (63). Monthly mean saturation vapor pressure (e_s) is calculated from mean daily maximum and minimum temperature (T_{max} and T_{min}, respectively), resulting in maximum and minimum saturation vapor pressure values (e_{s_max} and e_{s_min}, respectively). Monthly mean e_s is calculated as the mean of e_{s_max} and e_{s_min}. Monthly mean VPD is calculated as e_s minus e.

Daily meteorological fields are used to calculate ERC, FWI, KBDI, and FFDI. ERC is an output of the US national fire danger rating system and represents the potential daily fire intensity for a static fuel type [we use model G (65), which is dense conifer with heavy fuels] exposed to the cumulative drying effect on the 100- and 1,000-h fuels forced by temperature, precipitation, relative humidity, and solar radiation (66). The FWI is an output of the Canadian forest fire danger rating system that integrates several fire danger indices to provide a numerical rating of frontal fire intensity that accounts for fuel dryness and potential fire spread. KBDI is a proxy for the cumulative soil moisture deficit calculated using precipitation, temperature, and latitude. The FFDI is an empirical approach for assessing fire danger developed in Australia that uses temperature, wind speed, humidity, and a drought factor (67, 68). To accommodate the requirements of ERC and FWI that incorporate observations at 1300 and 1200 local standard time, respectively, we use daily T_{max} and minimum relative humidity. Each fire danger index has different input requirements and sensitivities to changes in individual meteorological variables. For example, wind speed has no impact on calculated ERC or KBDI, but does impact FWI and FFDI.

We repeated our analyses using the European Centre for Medium-Range Weather Forecasts Re-Analysis Interim (ERA-INTERIM) and National Centers for Environmental Prediction–National Center for Atmospheric Research (NCEP–NCAR) reanalysis products to assess structural uncertainty in observations and the resultant impact on our study. Reanalyses from ERA-INTERIM and NCEP–NCAR are acquired at 0.75- and 2.5-degree spatial resolution, respectively. Daily maximum and minimum relative humidity are not readily available from reanalysis, and are instead estimated using daily mean specific humidity (or dewpoint temperature) and maximum and minimum temperature (69). Any biases in estimated relative humidity imparted by this approach should not substantially impact calculated trends. Forest or woodland cover from the Environmental Site Potential product of LANDFIRE are aggregated up to the native resolution of ERA-INTERIM, where ERA-INTERIM grid cells are considered forested if composed of at least 50% woodland or forest. To maintain relatively similar spatial coverage across reanalysis products, we bilinearly interpolate aggregated forest cover from the ERA-INTERIM grid to the NCEP–NCAR grid.

Fig. S7 *A* and *B* shows linear least squares trends in 250-hPa geopotential height and precipitation for 1979–2015 for Mar–May and Jun–Sep. Geopotential height trends are computed using data from ERA-INTERIM reanalysis products. Seasonal precipitation trends are computed using data from PRISM (product version AN81m: M3) (51).

Annual time series of standardized fuel aridity indices, number of days per year of high fire danger, and fire weather season length aggregated for western US forested areas, both based on observations and based on observations after exclusion of the anthropogenic climate signal are provided in Supplemental Datasets S1–S3.

Fire Data

Satellite derived burned area for 1984–2014 are obtained from the Monitoring Trends in Burn Severity (MTBS; ref. 70). This record consists of only large wildfires at least 404 ha in size, but these fires account for over 92% of the total burned area in forests across the western United States (2). Area burned for 2015 is estimated using the MODIS burned area product version 5.1 (71). MODIS annual burned-area values were bias corrected to the MTBS record across the overlap period (2001–2014). Annual records of the logarithm of western US forest fire area derived from MTBS and MODIS were highly correlated ($r = 0.97$, $P < 0.01$) during the overlap period.

Climate Models

We obtained monthly means of daily 2-m T_{max} (*tasmax*), T_{max} (*tasmin*), specific humidity (*huss*), and surface pressure (*ps*) from available ensemble members of 27 GCMs participating in the fifth phase of the Climate Model Intercomparison Project (Table S3). We appended historical model simulations for 1850–2005 with simulations for experiment RCP8.5 for 2006–2099 (72). CMIP5 models were used to obtain an anthropogenic climate signal that could be removed from the observational record. In addition, we evaluated CMIP5 trends in seasonal precipitation (*pr*) and 250-hPa geopotential height (gz_{250}) for 39 models to evaluate the magnitude of anthropogenic impacts on precipitation during 1979–2015 relative to observed trends during this period.

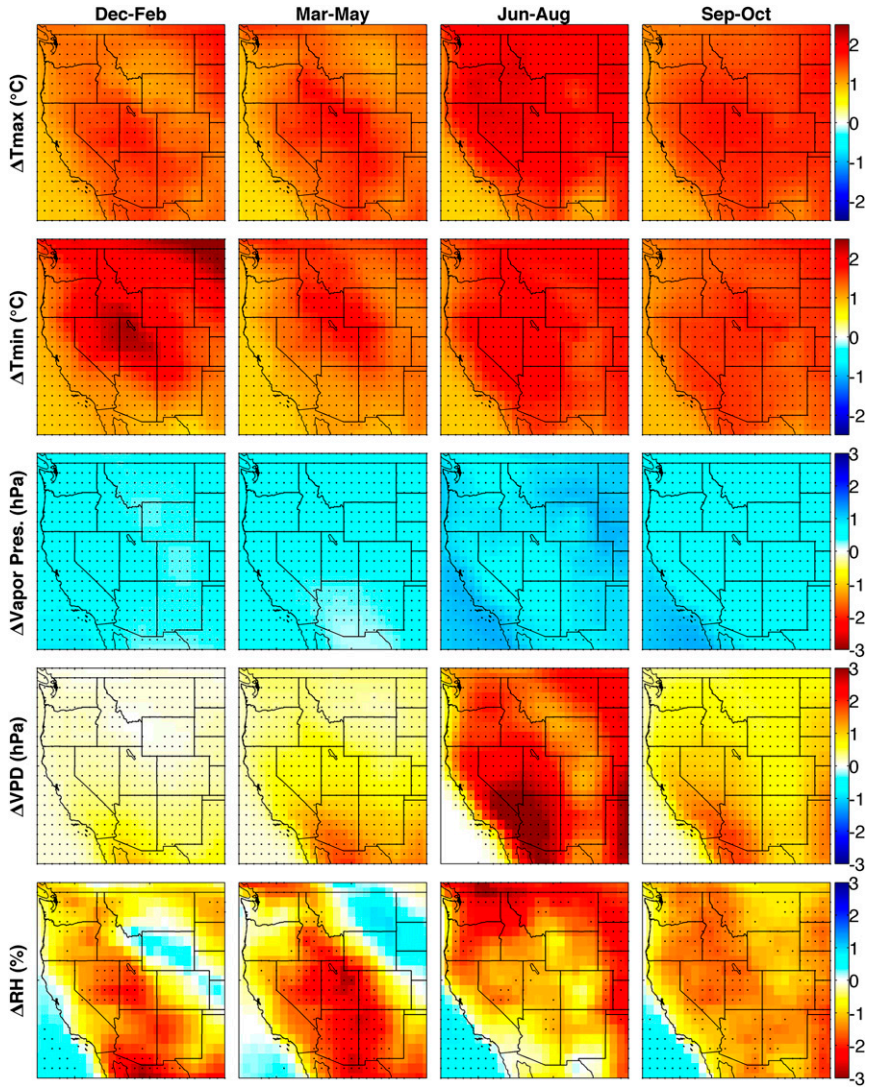

Fig. S1. Multimodel mean anthropogenic climate change signal of 50-y smoothed values for 2015 minus those for 1901 for (*Left* to *Right*) Dec–Feb, Mar–May, Jun–Aug, and Sep–Nov for (*Top* to *Bottom*) maximum temperature, minimum temperature, vapor pressure, vapor pressure deficit, mean relative humidity, maximum relative humidity, and minimum relative humidity. Black dots show grid cells where at least 20 (>74%) of the 27 models agree on the direction of the trend.

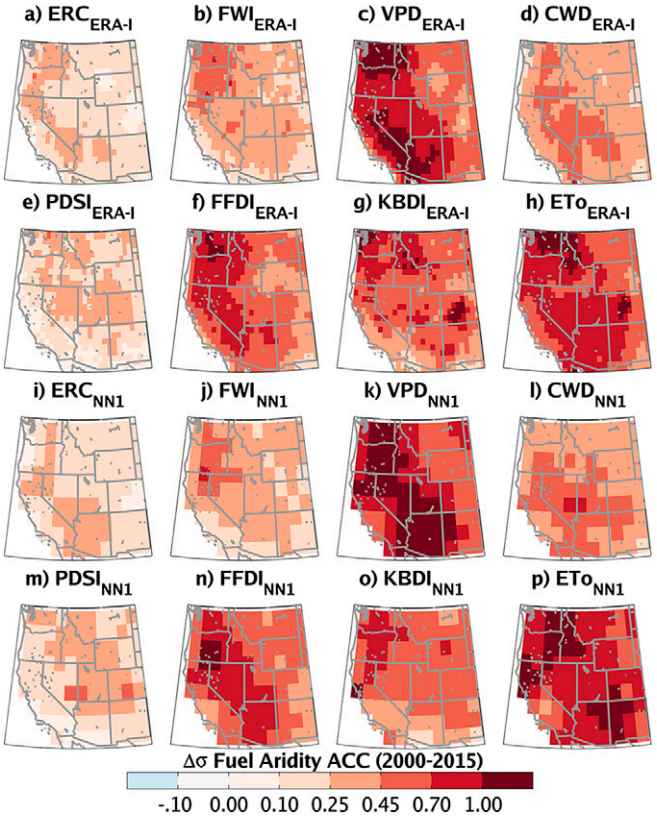

Fig. S2. As in Fig. 2 but for (*A*–*H*) ERA-INTERIM and (*I*–*P*) NCEP–NCAR reanalysis. The influence of ACC on fuel aridity during 2000–2015 is shown by the difference between standardized fuel aridity metrics calculated from observations and those calculated from observations excluding the ACC signal. The sign of PDSI is reversed for consistency with other aridity measures.

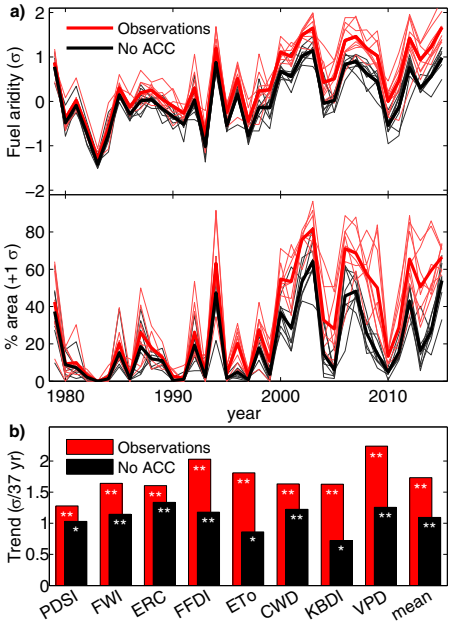

Fig. S3. As in Fig 3 but for ERA-INTERIM. (*A*) Time series of (*Top*) standardized annual fuel aridity metrics and (*Bottom*) percent of forest area with standardized fuel aridity exceeding one SD. Red lines show observations and black lines show records after exclusion of the ACC signal. Only the four monthly metrics extend back to 1950. Daily fire danger indices are constrained to 1979–2015. Bold lines indicate averages across fuel aridity metrics. (*B*) Linear trends in the standardized fuel aridity metrics during 1979–2015 for (red) observations and (black) records excluding the ACC signal (black). Asterisks indicate positive trends at the (*) 95% and (**) 99% significance levels.

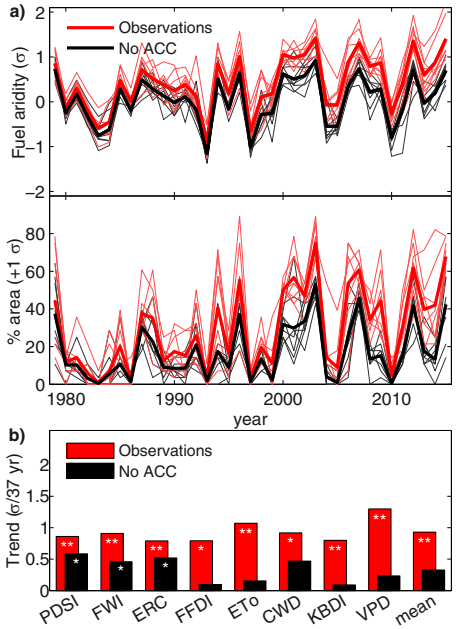

Fig. S4. As in Fig 3 but for NCEP–NCAR reanalysis. (*A*) Time series of (*Top*) standardized annual fuel aridity metrics and (*Bottom*) percent of forest area with standardized fuel aridity exceeding one SD. Red lines show observations and black lines show records after exclusion of the ACC signal. Only the four monthly metrics extend back to 1950. Daily fire danger indices are constrained to 1979–2015. Bold lines indicate averages across fuel aridity metrics. (*B*) Linear trends in the standardized fuel aridity metrics during 1979–2015 for (red) observations and (black) records excluding the ACC signal (black). Asterisks indicate positive trends at the (*) 95% and (**) 99% significance levels.

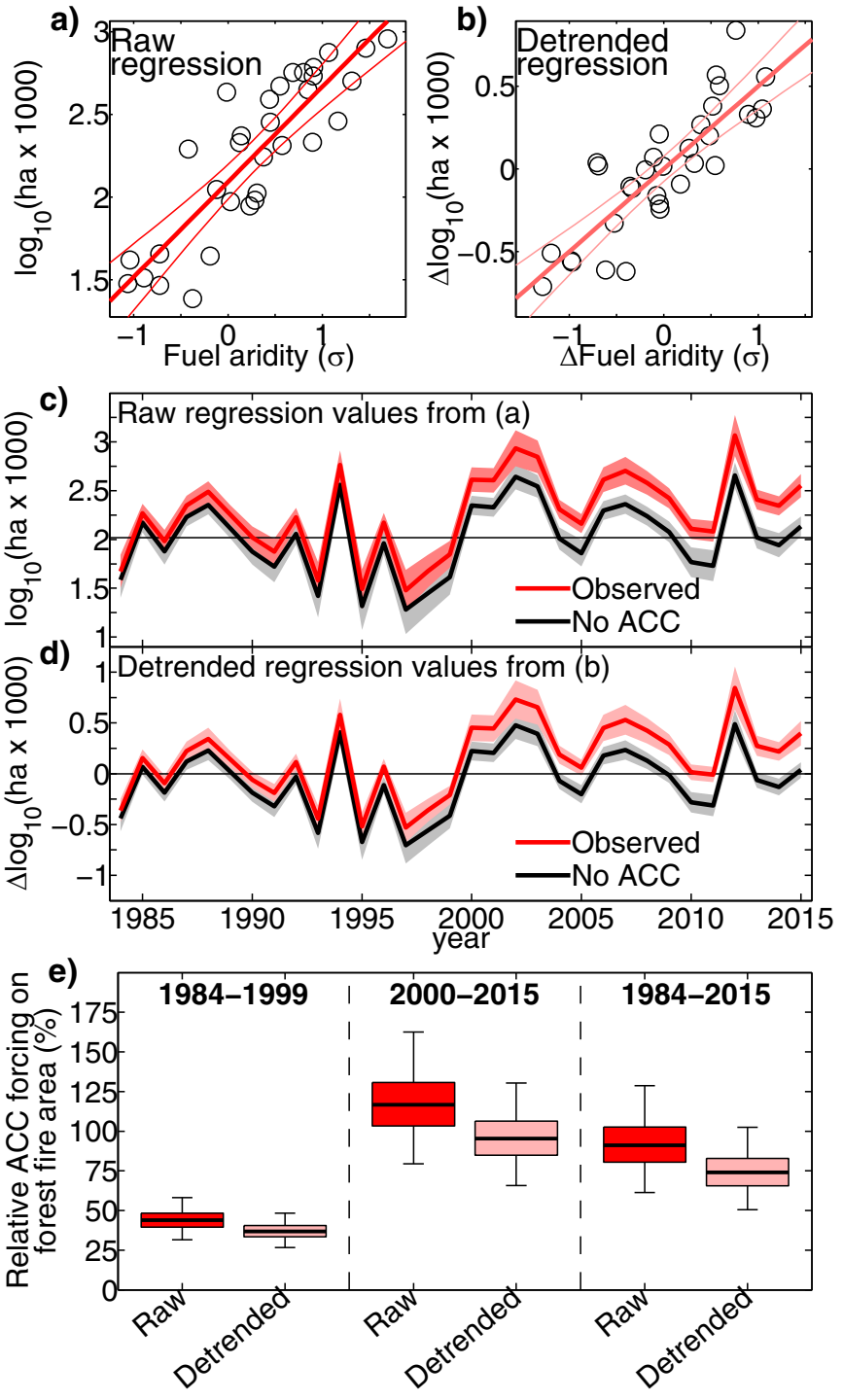

Fig. S5. Relationships between all-metric mean fuel aridity anomalies and burned area in western US forests (*A* and *B*) are used to model the annual response of forest fire area to fuel aridity (*C* and *D*) under observed fuel aridity conditions and those recalculated after the removal of ACC. Two methods are used to derive the response of forest fire area: (*A*) derived from raw data (as presented in the article) and (*B*) derived from detrended data for 1984–2015. This alternate approach is more conservative because it reduces risk of assuming an artificially strong relationship caused by common but unrelated trends. (*E*) The estimated relative forcing of ACC on cumulative burned area, calculated as the relative difference between burned area modeled from observed fuel aridity and burned area modeled in the absence of ACC. In *A*–*D*, areas bounding the central lines correspond to 95% confidence intervals around the regression lines. In *E*, boxes and whiskers indicate 50% and 95% confidence intervals, respectively.

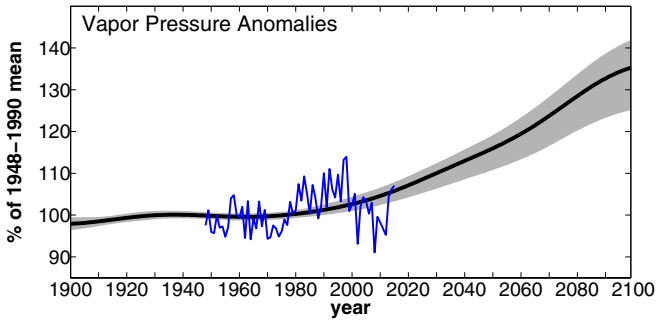

Fig. S6. Observations (blue) versus CMIP5 projections (black and gray) of March–September vapor pressure anomalies (relative to 1948–1990 mean) in western US forest areas. Thick black line is the multimodel ($n = 27$) mean and gray area bounds the interquartile values. CMIP5 projections have had a 50-y low-pass filter applied to exclude high-frequency variations caused by natural climate variability.

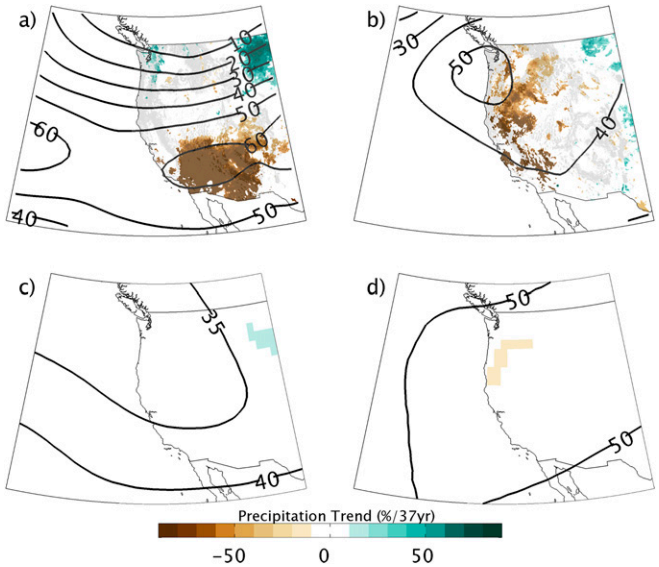

Fig. S7. Linear trend in (*A*) March–May, and (*B*) June–September (contours) 250-hPa geopotential height (in meters, data source: ERA-INTERIM) and (background) precipitation (percent of 1979–2015 average, data source: PRISM an81m) during 1979–2015. Only precipitation trends significant at the $P < 0.1$ level are shown. *Lower* shows CMIP5 ensemble-mean trends for the same variables during 1979–2015 for (*C*) March–May and (*B*) June–September ($n = 39$ models). For precipitation, trends are only shown if at least 75% of models agree on the sign of the trend. Trends are reported in units per 37 y. The location of western US forests is shown in gray in *A* and *B*.

Table S1. Pearson's correlation coefficients between standardized fuel aridity metrics and log-10 area burned (1984–2015), and linear change in in the standardized duel aridity metrics during 1979–2015

Metric	gridMET	No ACC gridMET	ERA–I	No ACC ERA–I	NN1	No ACC NN1
Interannual correlation with log–10 of area burned						
PDSI	–0.76**	–0.71**	–0.74**	–0.72**	–0.72**	–0.67**
FWI	0.80**	0.71**	0.87**	0.86**	0.75**	0.69**
ERC	0.87**	0.85**	0.86**	0.85**	0.75**	0.71**
FFDI	0.83**	0.74**	0.86**	0.85**	0.76**	0.64**
ETo	0.81**	0.65**	0.82**	0.73**	0.71**	0.54**
CWD	0.87**	0.81**	0.87**	0.85**	0.78**	0.72**
KBDI	0.80**	0.74**	0.79**	0.73**	0.73**	0.60**
VPD	0.87**	0.77**	0.83**	0.81**	0.75**	0.60**
MEAN	0.87**	0.79**	0.87**	0.85**	0.80**	0.70**
Linear trend in standardized fuel aridity metric per 37 years						
PDSI	–1.12*	–0.75	–1.28**	–1.03**	–0.86**	–0.59*
FWI	0.79*	0.25	1.64**	1.15**	0.91**	0.46*
ERC	1.30**	0.93**	1.61**	1.34**	0.79**	0.52*
FFDI	1.04*	0.35	2.03**	1.18**	0.79*	0.10
ETo	1.45**	0.27	1.81**	0.86*	1.07**	0.16
CWD	1.30**	0.70	1.63**	1.22**	0.92*	0.47
KBDI	0.94**	0.49	1.63**	0.72*	0.80**	0.09
VPD	1.73**	0.58	2.24**	1.26**	1.30**	0.23
MEAN	1.21**	0.54	1.73**	1.10**	0.93**	0.33

Units of the trends are SDs per 37 y, as in Fig. 3. Columns labeled as "No ACC" indicate that these variables have been recalculated after subtraction of the CMIP5 ensemble-mean trends in temperature and vapor pressure. Correlations and trends are shown using the gridded meteorological dataset (gridMET) (50), ERA-INTERIM (ERA-I), and NCEP–NCAR (NN1). Asterisks indicate significance at the (*) 95% and (**) 99% levels. Significance was evaluated using a two-tailed test for correlations and a single-tailed test for trends.

Table S2. Linear trend in the relative fire weather season length and number of days of high fire potential (exceeding the 95th percentile of observations) per 37 y averaged over western forests from 1979 to 2015

Metric	gridMET	No ACC gridMET	ERA–I	No ACC ERA–I	NN1	No ACC NN1
Trend in fire weather season length (percent) per 37 years						
KBDI	50.0%*	20.7%	80.6**	37.3%*	13.7%	–4.2%
FFDI	37.1%*	7.9%	57.8%**	34.3%**	19.5%*	0.5%
FWI	33.6%*	9.3%	57.7%**	41.3%**	25.1%**	11.7%
ERC	45.1%**	38.4%**	45.3%**	40.5%**	19.5%**	16.6%*
MEAN	41.4%*	19.1%	60.4%**	38.3%**	19.5%*	5.8%
Trend in number of days with high fire potential per 37 years						
KBDI	12.7*	4.9	26.0**	10.0	11.3	–2.9
FFDI	15.1**	3.2	19.8**	8.0*	4.3	–4.2
FWI	11.7*	2.9	17.1**	11.2**	6.4*	2.7
ERC	28.4**	20.0**	32.2**	24.1**	10.7*	2.6
MEAN	17.0**	7.8	23.8**	13.3**	8.2*	–0.3

Columns labeled as "No ACC" indicate that these variables have been recalculated after subtraction of the CMIP5 ensemble-mean trends in temperature and vapor pressure. Trends are shown using the gridded meteorological dataset (gridMET) (50), ERA-INTERIM (ERA-I), and NCEP–NCAR (NN1). Asterisks indicate significant trends at the (*) 95% and (**) 99% levels. Significance was evaluated using a single-tailed test for trends.

Table S3. List of the 39 climate models from the CMIP5 used in the study

	Resolution	Variables		Ensemble size	
Name	lat x lon	*tasmax, tasmin, huss, ps*	*pr, gz_{250}*	Historical	rcp8.5
ACCESS1-0	1.25° x 1.875°	x	x	3	1
ACCESS1-3	1.25° x 1.875°	x	x	3	1
BCC-CSM1-1-M	1.1215° x 1.125°	x	x	3	1
BCC-CSM1-1	2.7905° x 2.8125°	x	x	3	1
BNU-ESM	2.7905° x 2.8125°		x	1	1
CANESM2	2.7905° x 2.8125°	x	x	5	5
CCSM4	0.9424° x 1.25°	x	x	8	6
CESM1-BGC	0.9424° x 1.25°	x	x	1	1
CESM1-CAM5	0.9424° x 1.25°	x	x	3	3
CESM1-WACCM	1.8947° x 2.5°	x	x	7	3
CNRM-CM5	1.4008° x 1.4063°	x	x	10	5
CSIRO-MK3-6–0	1.8652° x 1.875°	x	x	10	10
CMCC-CESM	3.711° x 3.75°		x	1	1
CMCC-CM	0.7484° x 0.75°		x	1	1
CMCC-CMS	1.8652° x 1.875°		x	1	1
FGOALS-G2	2.7905° x 2.8125°		x	5	1
FIO-ESM	2.7905° x 2.8125°		x	3	3
GFDL-CM3	2° x 2.5°	x	x	5	1
GFDL-ESM2G	2.0225° x 2.5°	x	x	1	1
GFDL-ESM2M	2.0225° x 2.5°	x	x	1	1
GISS-E2-H	2° x 2.5°	x	x	18	5
GISS-E2-R	2° x 2.5°	x	x	24	5
GISS-E2-H-CC	2° x 2.5°		x	1	1
GISS-E2-R-CC	2° x 2.5°		x	1	1
HADGEM2-CC	1.25° x 1.875°	x	x	3	3
HADGEM2-ES	1.25° x 1.875°	x	x	5	4
INMCM4	1.5° x 2°	x	x	1	1
IPSL-CM5A-LR	1.8947° x 3.75°	x	x	6	4
IPSL-CM5A-MR	1.2676° x 2.5°	x	x	3	1
IPSL-CM5B-LR	1.8947° x 3.75°	x	x	1	1
MIROC-ESM-CHEM	2.7905° x 2.8125°	x	x	1	1
MIROC-ESM	2.7905° x 2.8125°	x	x	3	1
MIROC5	1.4008° x 1.4063°	x	x	5	3
MRI-CGCM3	1.1215° x 1.125°	x	x	5	1
MPI-ESM-LR	1.8652° x 1.875°		x	3	3
MPI-ESM-MR	1.8652° x 1.875°		x	3	1
MRI-ESM1	1.1215° x 1.125°		x	1	1
NORESM1-M	1.8947° x 2.5°	x	x	3	1
NORESM1-ME	1.8947° x 2.5°		x	1	1

All of these models had monthly output for precipitation (*pr*) and 250-hPa geopotential height (gz_{250}). The 27 models that had monthly mean output of daily 2-m T_{max} (*tasmax*), T_{min} (*tasmin*), specific humidity (*huss*), and surface pressure (*ps*) and denoted with an x in the third column. The number of ensemble realizations for the historical (1850–2005) and rcp8.5 (2006–2099) experiments are shown in the fifth and sixth columns, respectively.

Other Supporting Information Files

Dataset S1 (CSV)
Dataset S2 (CSV)
Dataset S3 (CSV)